Electronic Supplementary Material (ESI) for New Journal of Chemistry.

ELECTRONIC SUPPLEMENTARY INFORMATION

NEW PYRIDAZINE-BASED BINUCLEAR NICKEL(II), COPPER(II) AND ZINC(II) COMPLEXES AS PROSPECTIVE ANTICANCER AGENTS

Ummer Muhammed Rafi[a], Dharmasivam Mahendiran[a], Azees Khan Haleel[a], Rakesh Pandeet Nankar[b], Mukesh Doble[b] and Aziz Kalilur Rahiman*[a].

[a]Post-Graduate and Research Department of Chemistry, The New College (Autonomous), Chennai-600 014, India.

[b] Bioengineering and Drug Design Lab, Department of Biotechnology, Indian Institute of Technology Madras, Chennai-600 036, India.

Table S1 Selected bond lengths (Å) and bond angles (°) of the ligand HL^3.

Bonds lengths (Å)			
C(4)–N(4)	1.332(3)	C(12)–N(13)	1.505(4)
C(4)–N(3)	1.364(3)	C(14)–N(1)	1.449(3)
C(5)–N(2)	1.292(3)	C(14)–C(15)	1.520(4)
C(5)–C(6)	1.445(3)	N(2)–N(3)	1.387(3)
C(9)–N(1)	1.389(3)	N(3)–H(3A)	0.913(15)
C(11)–O(1)	1.361(3)	N(4)–N(5)	1.350
C(12)–N(1)	1.465(3)	O(1)–H(1)	0.8200
Bonds angles (°)			
N(5)–C(1)–C(2)	124.7(2)	N(1)–C(14)–C(15)	113.0(2)
N(4)–C(4)–N(3)	114.3(2)	C(9)–N(1)–C(14)	122.9(2)
N(4)–C(4)–C(3)	123.3(2)	C(9)–N(1)–C(12)	116.0(2)
N(2)–C(5)–C(6)	121.5(2)	C(5)–N(2)–N(3)	114.8(2)
C(11)–C(6)–C(5)	123.0(2)	C(4)–N(3)–N(2)	120.4(2)
C(7)–C(6)–C(5)	119.6(2)	C(4)–N(3)–H(3A)	117.1(14)
C(8)–C(9)–N(1)	121.1 (2)	N(2)–N(3)–H(3A)	115.7(14)
N(1)–C(9)–C(10)	120.1 (2)	C(4)–N(4)–N(5)	119.3(2)
O(1)–C(11)–C(6)	121.6 (2)	C(1)–N(5)–N(4)	118.8(2)
N(1)–C(12)–C(13)	112.3 (3)	C(11)–O(1)–H(1)	109.5

Table S2 Hydrogen bonds geometry for the ligand HL^3 (Å and °).

D–H···A	d (D–H)	d (H···A)	d(D···A)	<D–H···A
C(2)–H(2)···O(1)^{i}	0.93	2.48	3.390(3)	164.7
C(5)–H(5)···N(5)^{ii}	0.93	2.67	3.562(3)	160.9
O(1)–H(1)···N(2)	0.82	1.97	2.643(3)	146.3
N(3)–H(3A)···N(4)^{ii}	0.913(15)	2.054(16)	2.950(3)	167(2)

Symmetry code: (i) –x+1, –y+1, –z+1 (ii) –x, –y, –z+1

Table S3 Selected IR data of the ligands (HL^{1-3}) and complexes (**1-9**).

Compound	ν(NH)	ν(C=N)	ν(Ar−O)	ν(N=N)	ν(M−O)	ν(M−N)	ν (NO_3)
HL^1	3218	1628	1283	1533	–	–	–
HL^2	3208	1629	1290	1518	–	–	–
HL^3	3194	1631	1282	1535	–	–	–
1	3220	1610	1264	1555	540	442	1383
2	3219	1601	1257	1552	516	423	1384
3	3220	1604	1243	1544	556	421	1384
4	3224	1605	1250	1545	530	430	1384
5	3115	1612	1240	1546	563	444	1387
6	3212	1608	1249	1568	563	443	1384
7	3217	1615	1277	1551	535	453	1380
8	3208	1613	1251	1554	512	448	1384
9	3220	1603	1243	1539	568	454	1382

Table S4 Characteristic ^{1}H and ^{13}C NMR chemical shifts values (ppm) for the synthesized ligands HL^{1-3} in DMSO-d_6.

Ligands	CH=N		C_{Ar}–OH		C_{Ar}–NH	
	^{1}H NMR	^{13}C NMR	^{1}H NMR	^{13}C NMR	^{1}H NMR	^{13}C NMR
HL^{1}	8.43	140.76	11.63	156.44	10.17	158.86
HL^{2}	8.33	137.08	11.80	161.79	11.60	158.92
HL^{3}	8.23	143.89	11.27	158.53	10.18	158.42

Table S5 UV-Vis data of the synthesized ligands (HL^{1-3}) and complexes (**1-9**).

Compounds	Wavelength (λ), nm
HL^1	339
HL^2	336, 465
HL^3	371
1	263, 298, 418, 588
2	233, 301, 412, 594
3	311, 423, 572
4	275, 398, 437, 655
5	263, 372, 441, 650
6	308, 411, 611
7	338
8	326
9	319

Table S6 Photoluminescence (PL) data of ligands and metal(II) complexes.

Compounds	λ_{abs}		λ_{em}		Stoke's shift (eV)
	(nm)	(eV)	(nm)	(eV)	
HL^1	336	3.69	415	2.98	0.71
HL^2	336	3.69	439	2.82	0.87
HL^3	371	3.34	481	2.57	0.77
1	263	4.69	341	3.63	1.06
2	301	4.11	473	2.62	1.49
4	275	4.50	331	3.74	0.76
5	263	4.71	346	3.58	1.13
7	338	3.66	395	3.13	0.53
8	326	3.80	322	3.85	–

Table S7 Electrochemical data for the complexes (**1-6**) at anodic (oxidation) and cathodic potential (reduction) region.

Complexes	$^{1}E_{pc}$ (V)	$^{2}E_{pc}$ (V)	$^{1}E_{pa}$ (V)	$^{2}E_{pa}$ (V)
1	−0.391	−0.739	1.025	1.153
2	−0.463	−0.790	1.009	1.140
3	−0.362	−0.634	1.020	1.151
4	−0.366	−0.671	–	–
5	−0.380	−0.687	–	–
6	−0.323	−0.654	–	–

Table S8 B3LYP/GEN and B3LYP/LANL2DZ Bond lengths (Å) and Bond angles (°) of complexes **1, 3, 5** and **9**.

Parameters	Calculated								Experimental [14, 38]
	B3LYP/GEN				B3LYP/LANL2DZ				
	1	**3**	**5**	**9**	**1**	**3**	**5**	**9**	
Bond length (Å)									
M(1)-N(2)	2.02532	2.02721	2.02812	2.02691	2.11207	2.09831	2.10949	2.10019	2.1037(17)
M(1)-N(4)	2.05092	2.06190	2.05975	2.06493	2.05719	2.02309	2.00100	2.00687	2.0027(17)
M(1)-O(1)	2.00892	2.00987	2.00437	2.01332	1.83215	2.00127	1.82309	1.91207	1.902(3)
M(1)-O(2)	2.06217	2.05387	2.06436	2.05641	2.38701	2.50942	2.50922	2.30981	2.421(4)
M(2)-N(7)	2.02810	2.02712	2.02793	2.02742	2.01983	2.20873	2.00803	2.00123	2.1037(17)
M(2)-N(9)	2.05011	2.05213	2.06258	2.06110	2.10932	2.02072	2.01012	2.01098	2.0027(17)
M(2)-O(1)	2.01021	2.00123	2.01 074	2.00877	1.84503	1.91025	1.98020	1.87901	1.902(3)
M(2)-O(2)	2.06209	2.05321	2.06085	2.04501	2.40026	2.30298	2.44012	2.52012	2.421(4)
Bond angle (deg)									
N2-M1-N4	66.28	68.39	66.93	64.32	78.00	77.47	78.88	79.64	76.60(6)
N4-M1-O2	92.73	94.17	90.07	96.10	86.61	88.05	87.81	87.66	–
N2-M1-O1	131.85	128.03	125.62	126.16	121.63	120.37	121.59	120.74	–
O1-M1-O2	92.41	91.93	90.28	90.07	80.42	82.14	81.59	79.86	84.47(14)
O2-M2-N7	132.87	134.01	131.93	134.20	121.82	120.36	121.56	120.73	–
N7-M2-N9	89.41	87.55	86.91	86.35	78.41	77.04	79.00	79.86	76.60(6)
N9-M2-O1	96.72	100.87	102.59	101.27	84.02	83.09	84.15	88.39	–
O2-M2-O1	72.32	76.61	78.06	72.48	83.59	80.93	81.59	80.20	84.47(14)

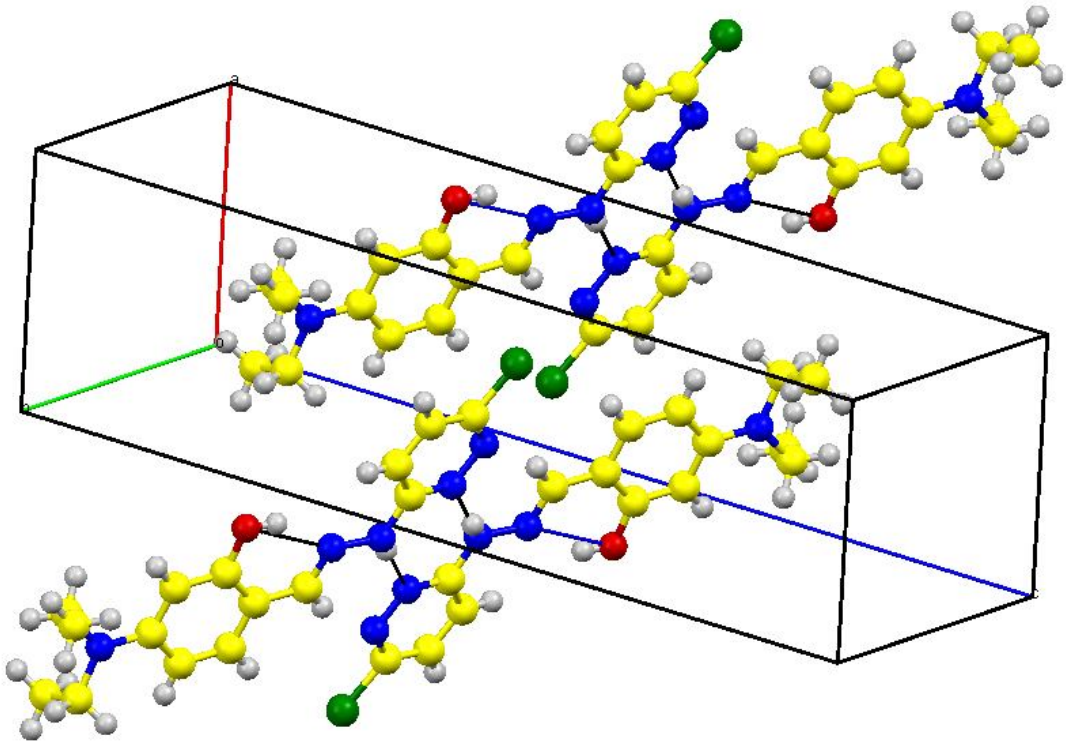

Fig. S1 Crystal packing diagram of ligand HL^3 projecting along the crystallographic *b*-axis.

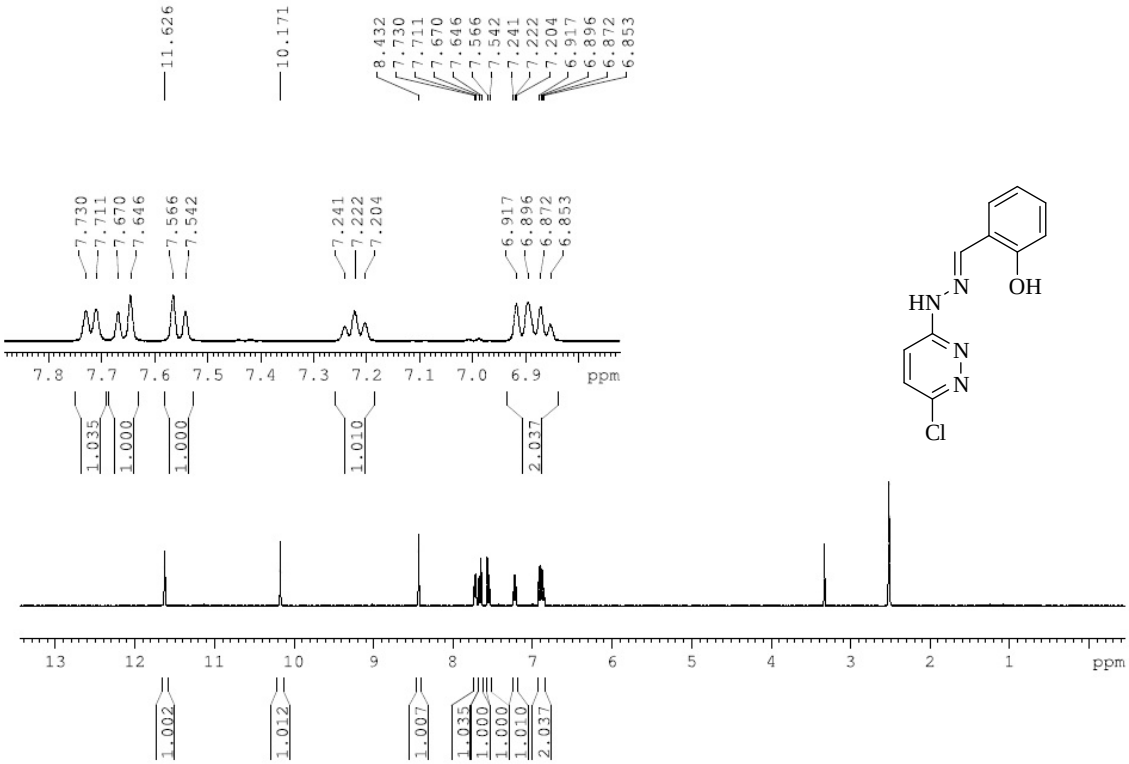

Fig. S2 ^{1}H NMR spectrum of the ligand HL^{1}.

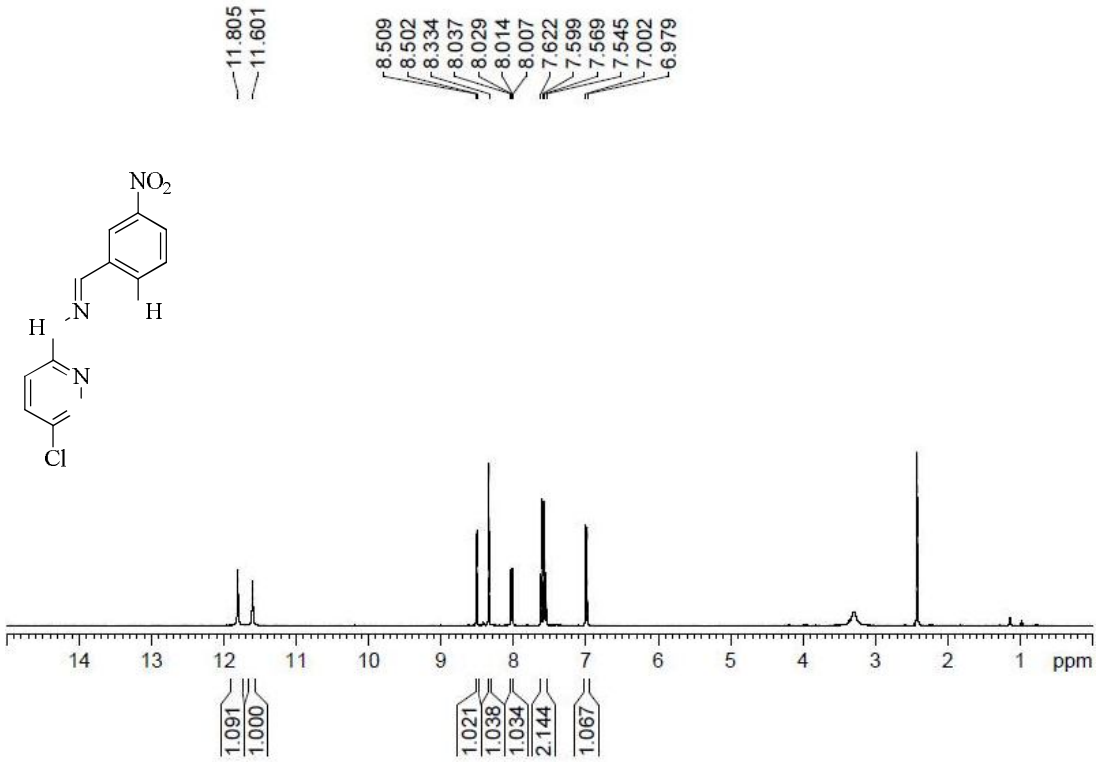

Fig. S3 ^{1}H NMR spectrum of the ligand HL^{2}.

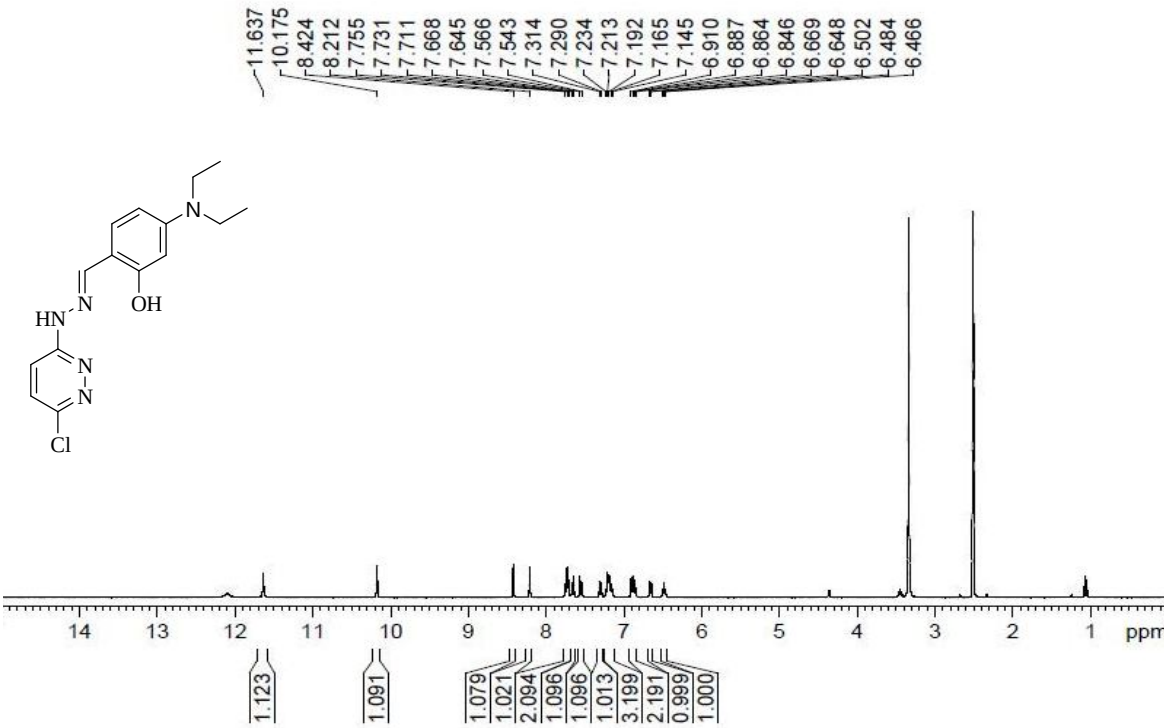

Fig. S4 ^{1}H NMR spectrum of the ligand HL^{3}.

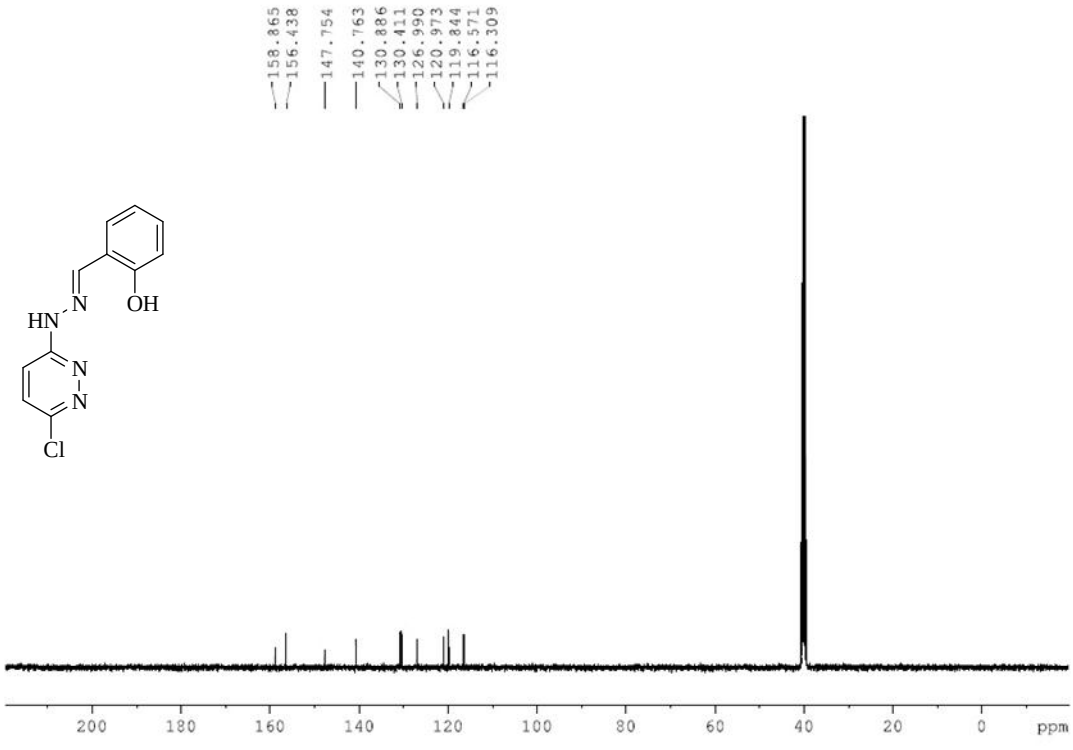

Fig. S5 ^{13}C NMR spectrum of the ligand HL^{1}.

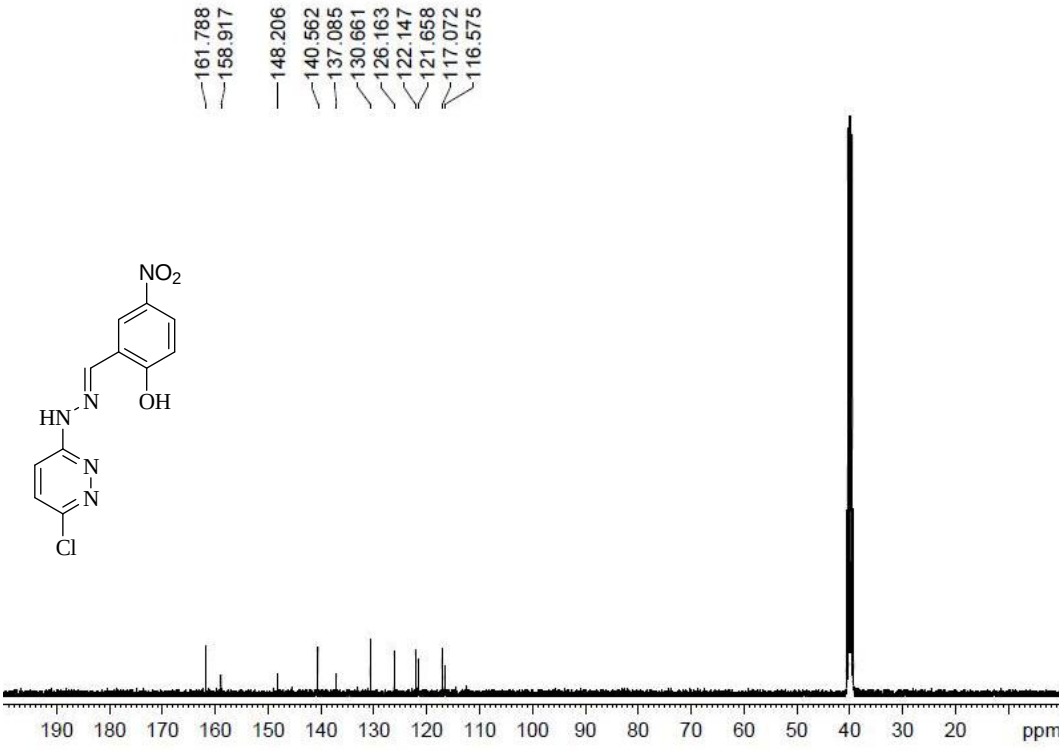

Fig. S6 ^{13}C NMR spectrum of the ligand HL^2.

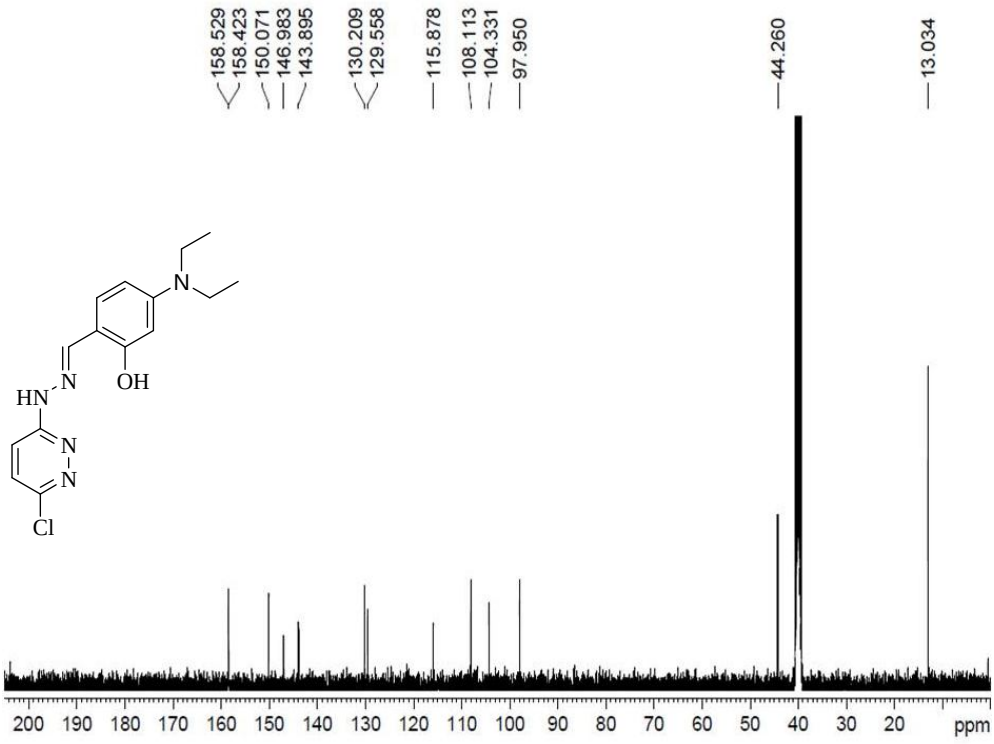

Fig. S7 ^{13}C NMR spectrum of the ligand HL^3.

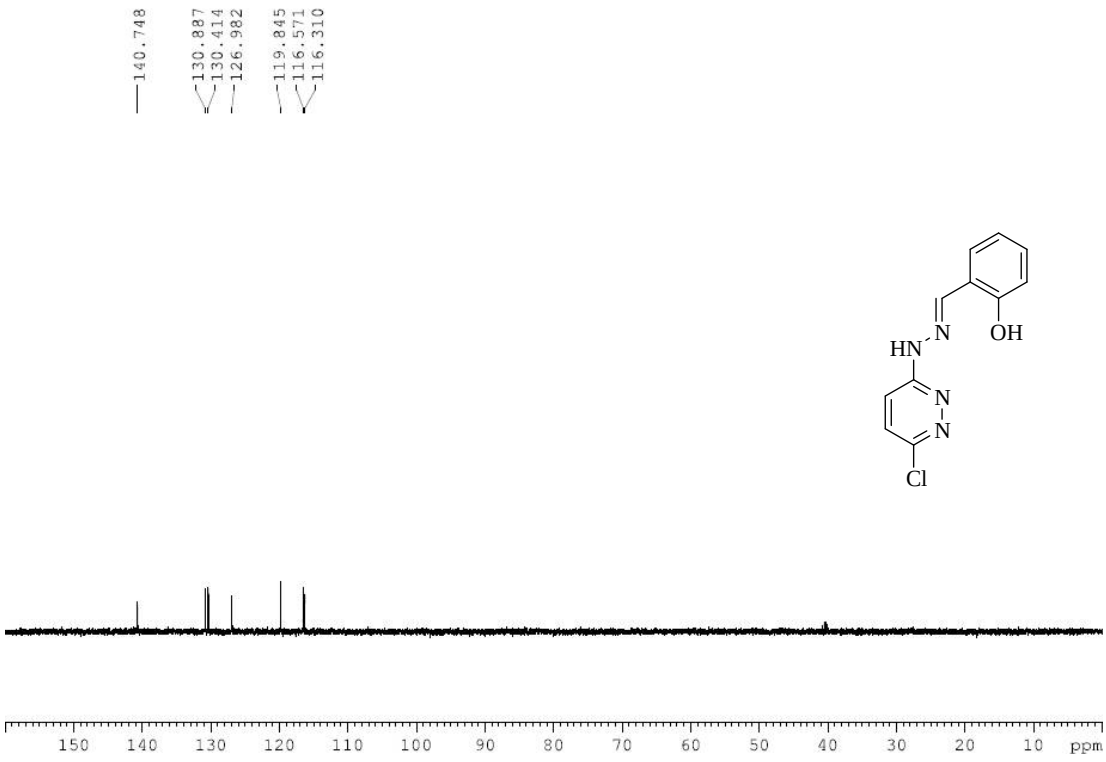

Fig. S8 ^{13}C DEPT-135 NMR spectrum of the ligand HL^{1}.

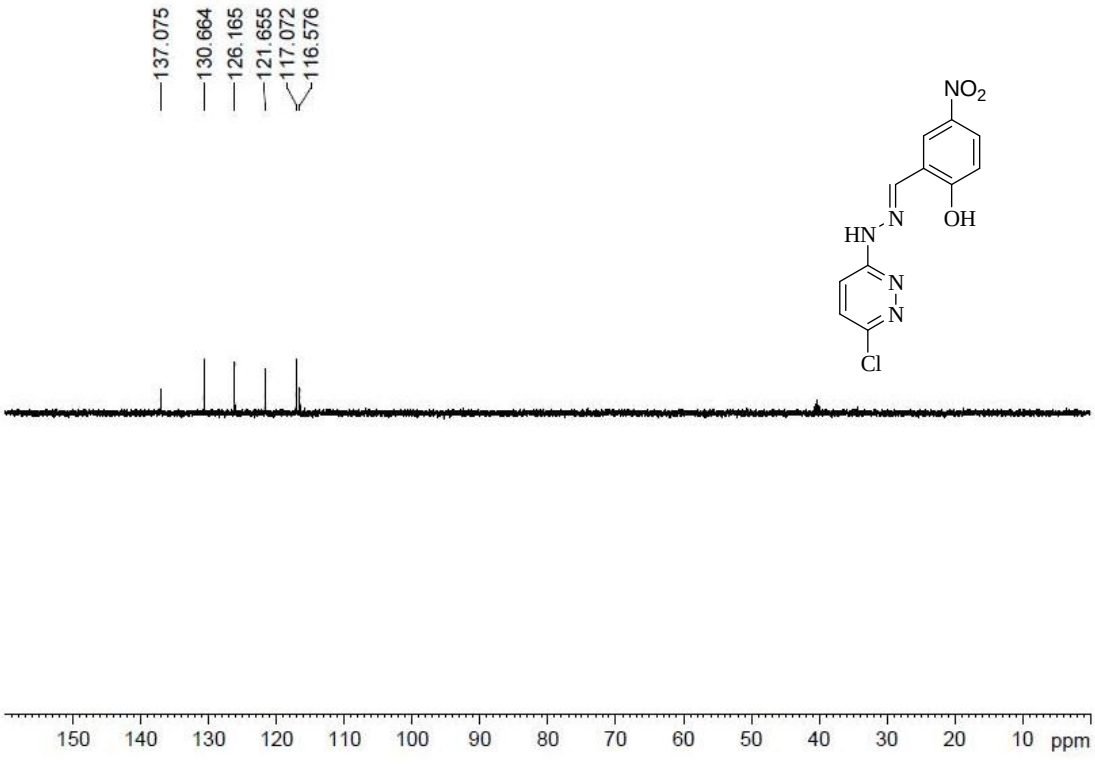

Fig. S9 ^{13}C DEPT-135 NMR spectrum of the ligand HL^{2}.

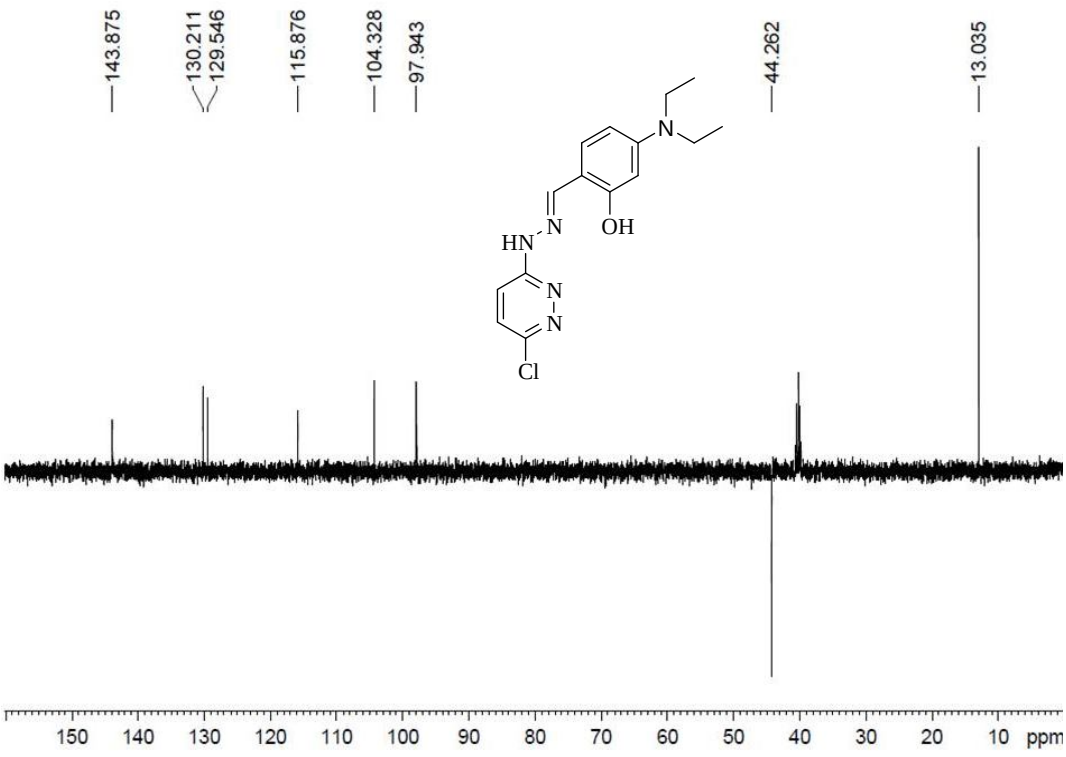

Fig. S10 ^{13}C DEPT-135 NMR spectrum of the ligand HL^3.

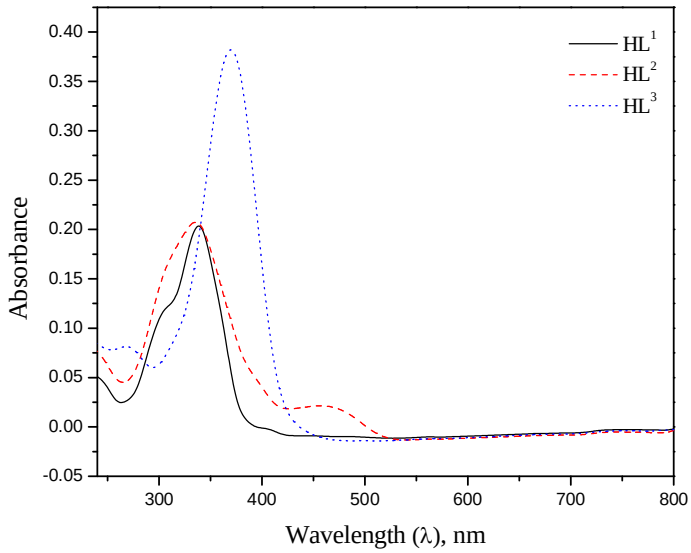

Fig. S11 UV-Vis spectra of the ligands HL^{1-3}.

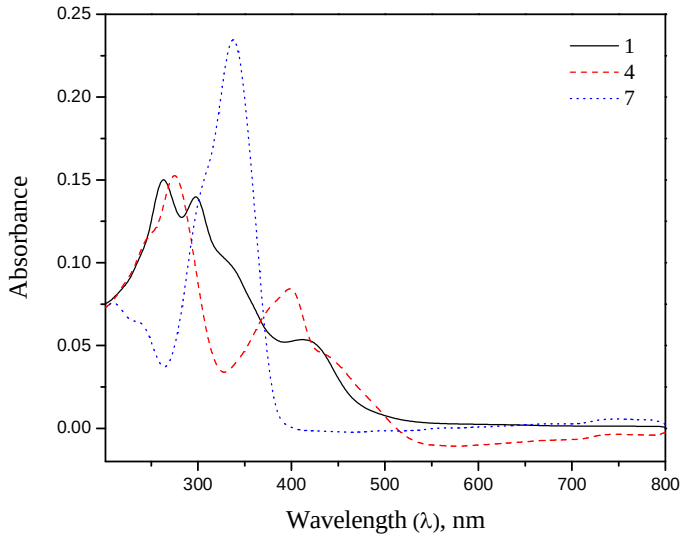

Fig. S12 UV-Vis spectra of the binuclear metal(II) complexes (**1**, **4** & **7**) of ligand HL^{1}.

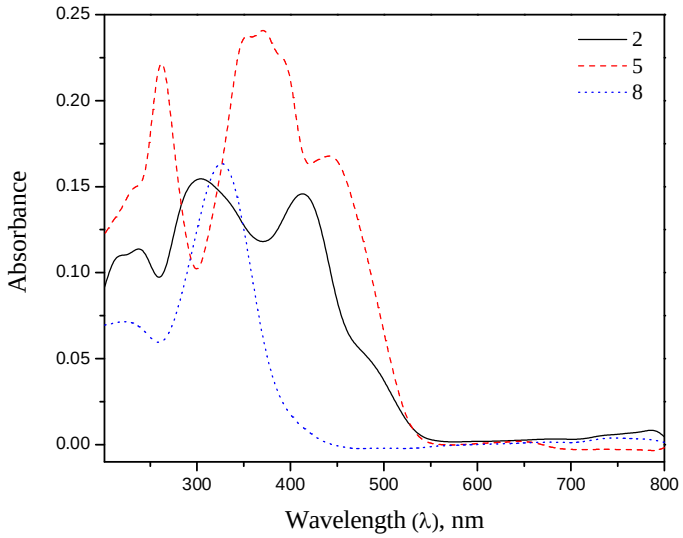

Fig. S13 UV-Vis spectra of the binuclear metal(II) complexes (**2**, **5** & **8**) of ligand HL^2.

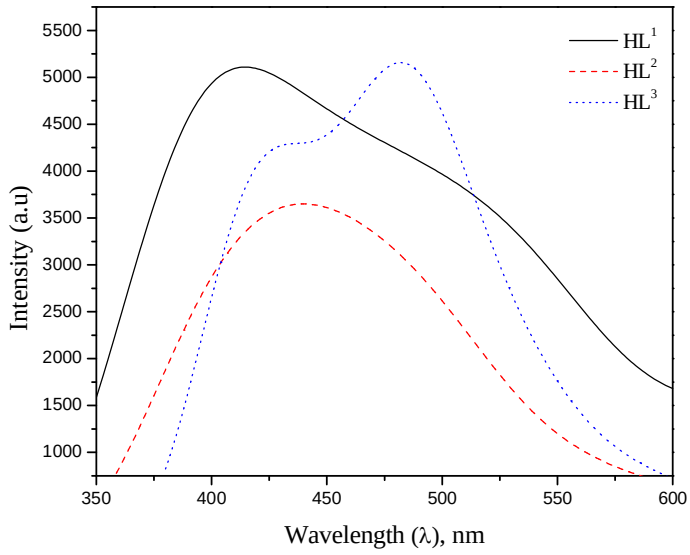

Fig. S14 Photoluminescence (PL) spectra of the ligands $HL^{1\text{-}3}$.

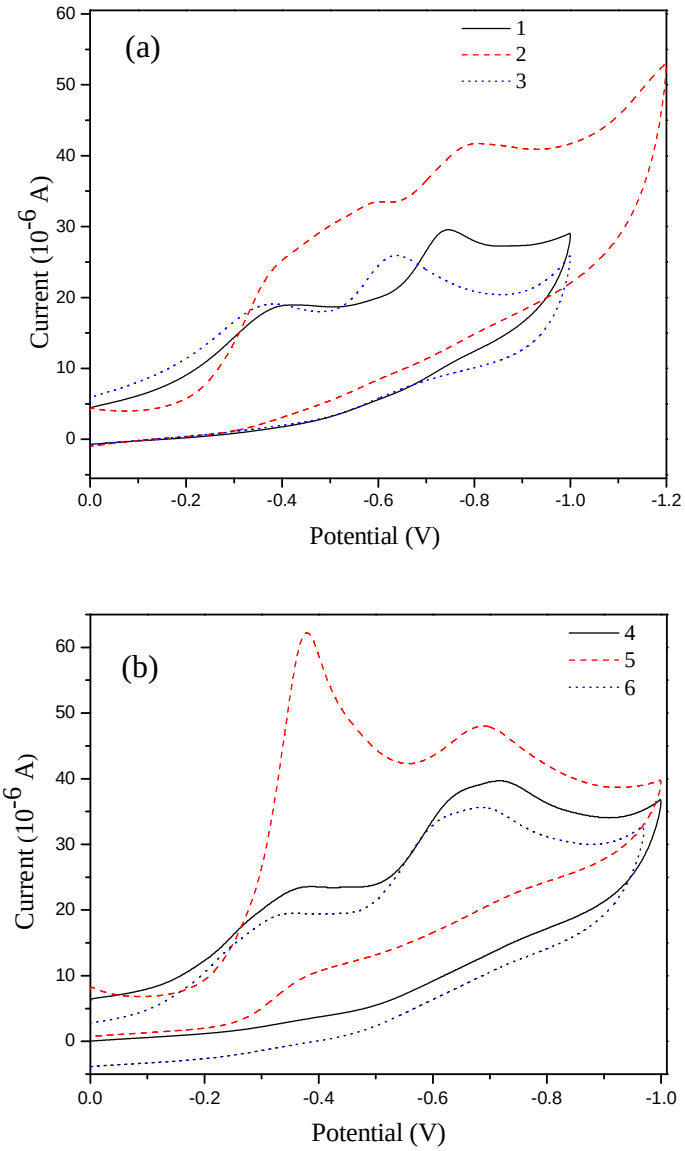

Fig. S15. Cyclic voltammograms of the binuclear nickel(II) (**1**-**3**) (a) and copper(II) (**4**-**6**) (b) complexes (Reduction process).

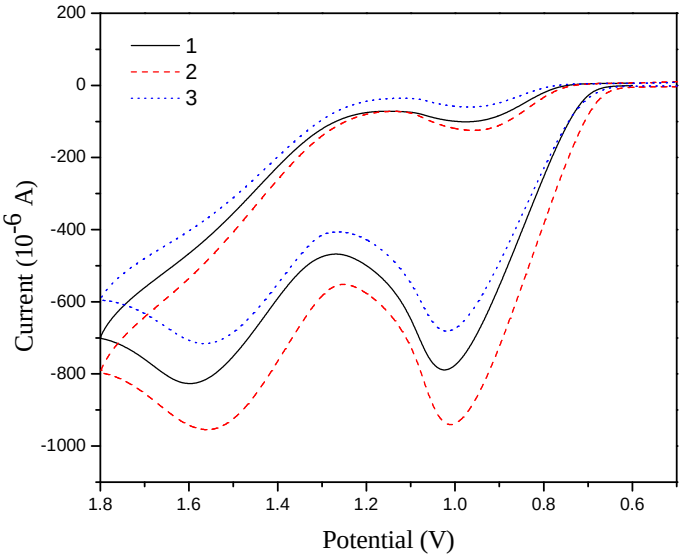

Fig. S16 Cyclic voltammograms of the binuclear nickel(II) complexes (**1**-**3**) (Oxidation process).

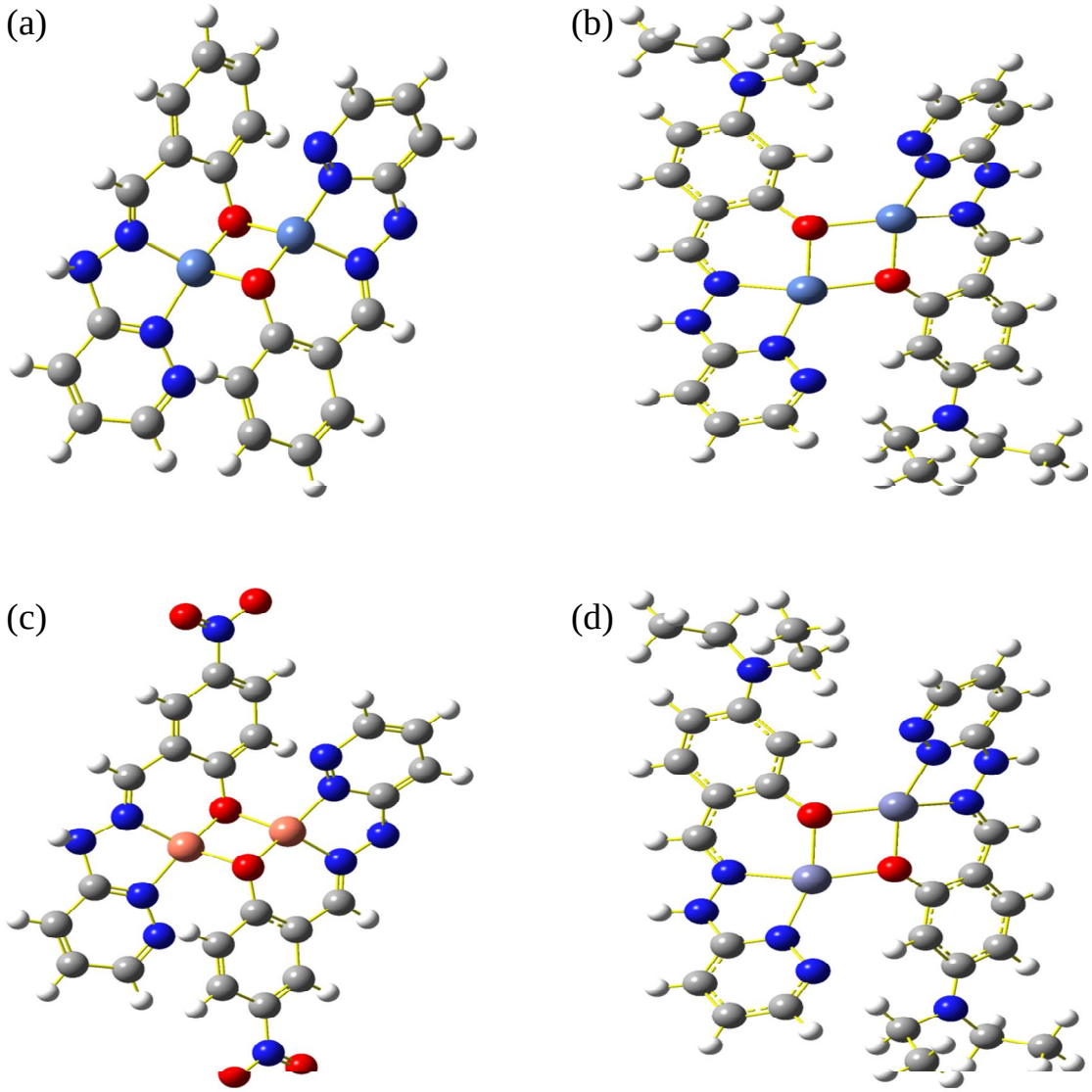

Fig. S17 Optimized geometry of the complexes **1** (a), **3** (b), **5** (c) and **9** (d).

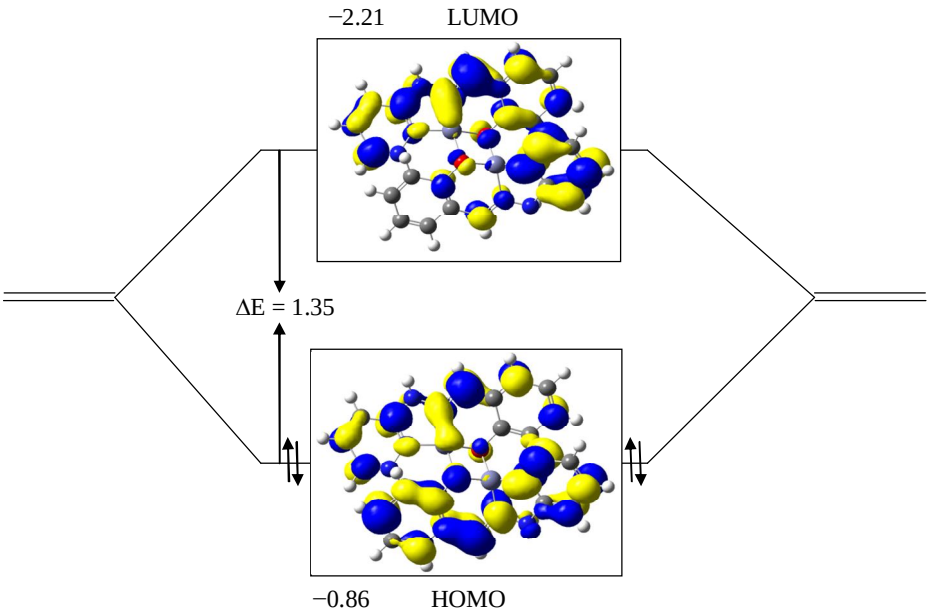

Fig. S18 Frontier molecular orbitals of the complex **7**.

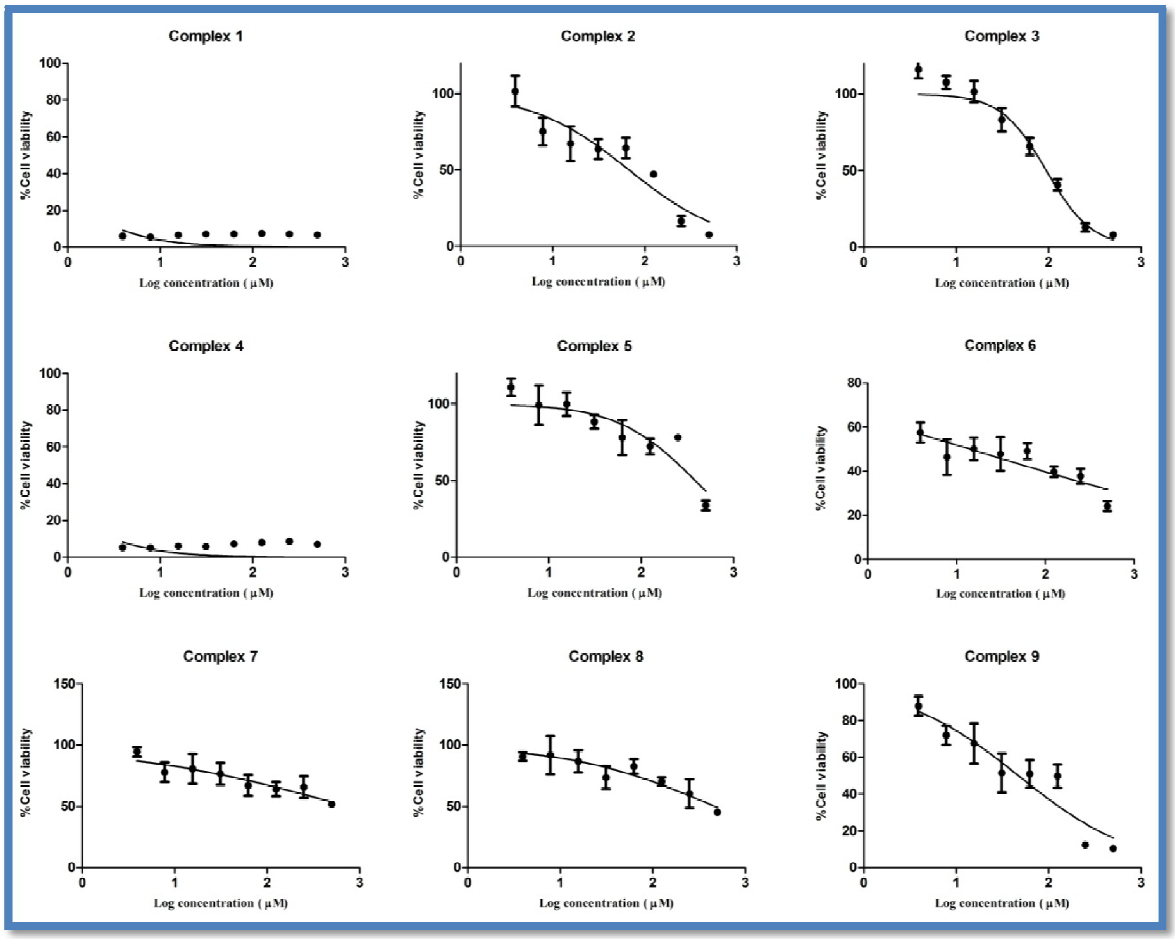

Fig. S19 Effect of pyridazine-based binuclear metal(II) complexes (**1**-**9**) on L6 cell viability.

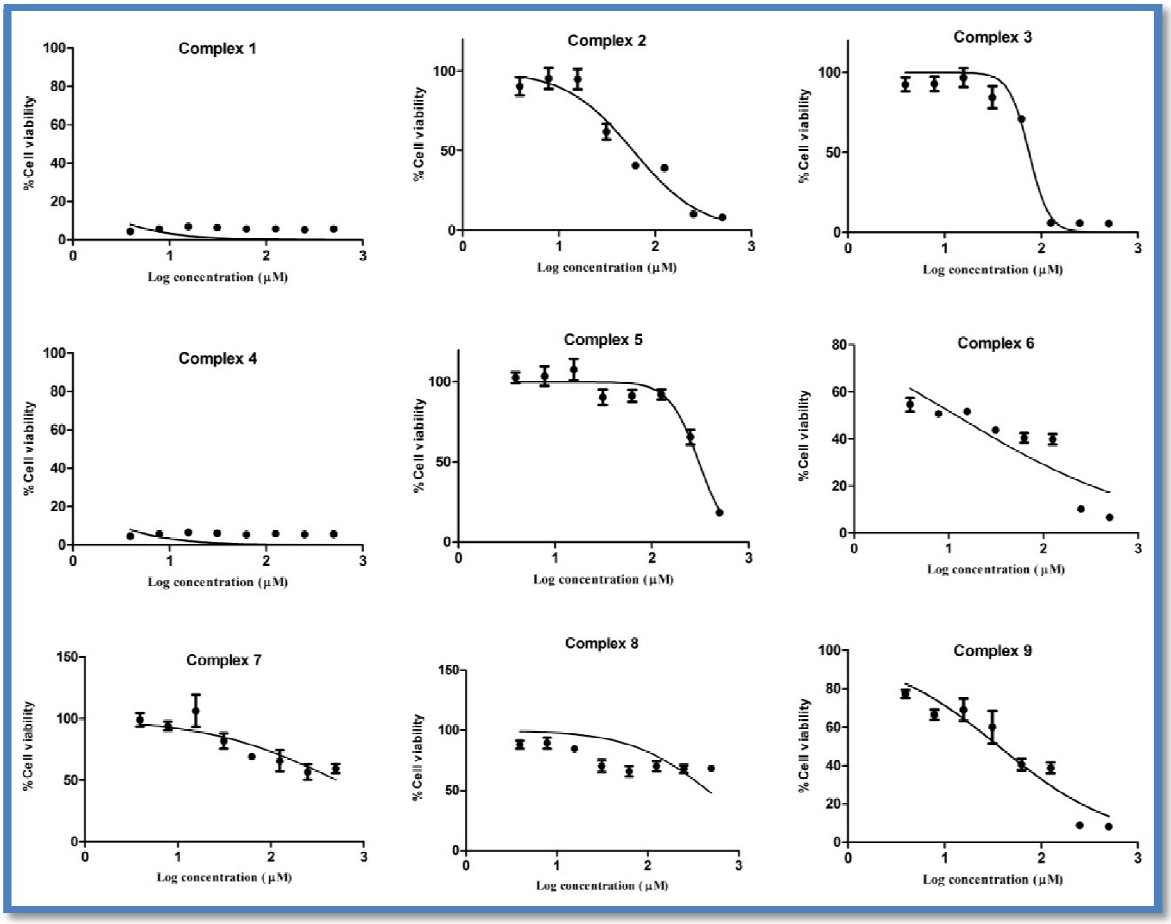

Fig. S20 Effect of pyridazine-based binuclear metal(II) complexes (**1**-**9**) on MDA-MB-231 cell viability.

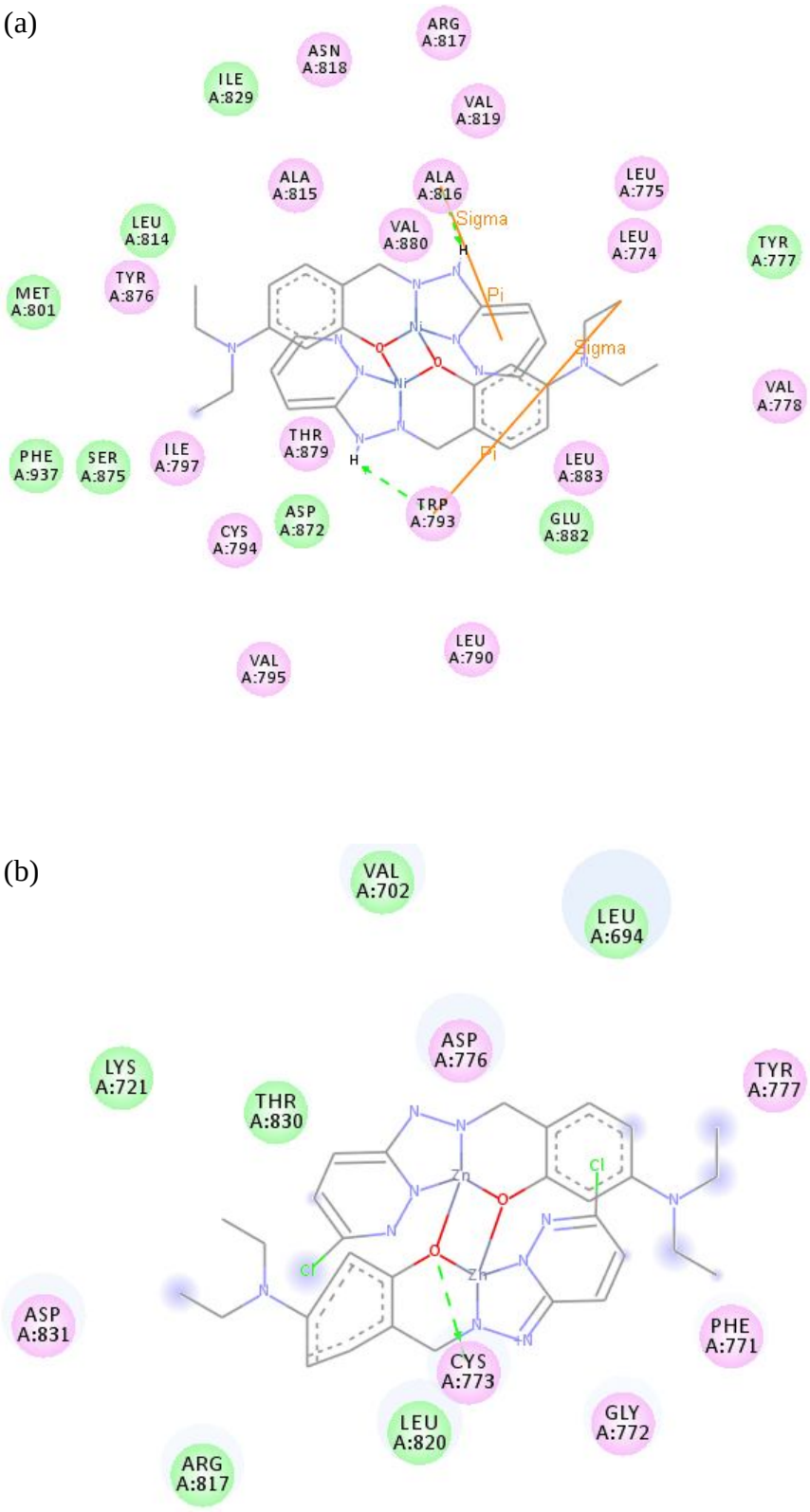

Fig. S21 Non-bonding interaction diagrams of complexes **3** (a) and **9** (b) docked with epidermal growth factor receptor (EGFR).